IEEE Access
Multidisciplinary ⋮ Rapid Review ⋮ Open Access Journal

Received 14 September 2023, accepted 29 September 2023, date of publication 2 October 2023,
date of current version 10 October 2023.

Digital Object Identifier 10.1109/ACCESS.2023.3321581

RESEARCH ARTICLE

Maximum Power Tracking for Centralized Temperature Difference Power Generation System Based on Elman Neural Network Combined With Improved Sparrow Search

XINYING HE, YAN CHEN, QIAN DU, AND LULU FENG
College of Electrical and Power Engineering, Taiyuan University of Technology, Taiyuan, Shanxi 030024, China

Corresponding author: Yan Chen (chenyan@tyut.edu.cn)

This work was supported in part by the Fundamental Research Project of Shanxi Provincial Department of Science and Technology under Grant 202203021211175, and in part by the Shanxi Scholarship Council of China under Grant 2020-039.

ABSTRACT Since the thermoelectric generation (TEG) sheets will be placed in places with different temperature gradients, it leads to multiple peaks in the duty-power (D-P) characteristic curve of a centralized TEG system under non-uniform temperature distribution (NTD). For this reason, this paper proposes an ENN-ISSA control algorithm, which combines the Elman neural network (ENN) with the sparrow search algorithm (SSA) by adding firefly perturbation. The ENN obtains the centralized TEG system's single-input and single-output fitting curves, after which the firefly perturbation is introduced into the SSA algorithm. Then the improved SSA algorithm is used to realize the maximum power point tracking (MPPT) control based on the fitted curves. Based on building a centralized TEG system Simulink model and analyzing the output characteristics of the TEG module, temperature constancy experiments, temperature change experiments, and accuracy analysis were conducted. The results of these simulation experiments all show that the algorithm can track the global maximum power point (GMPP) quickly and accurately in the duty-power (D-P) curve with multiple peaks compared with the perturbation observation method and particle swarm algorithm.

INDEX TERMS Centralized thermoelectric generation system, sparrow search algorithm, thermoelectric generator, Elman neural network, centralized maximum power point tracking.

I. INTRODUCTION

Fossil fuels produce a large amount of greenhouse gases during the combustion process, which not only cause global warming but also jeopardize human health [1], [2]. To alleviate the energy crisis and reduce environmental pollution, we should seek cleaner and renewable energy sources [3]. Thermoelectric Generation (TEG) is a new energy generation technology using semiconductor materials as the power generation carrier, which can convert medium and low-taste industrial waste heat into electricity without polluting the environment during the energy conversion process. Also, it has the advantages of being renewable, noiseless, easy to maintain, and climate independent [4]. Since the output voltage of a single TEG module is only a few volts and the output power is only a few tenths of a watt, TEG systems usually comprise multiple TEG modules connected in series and parallel to meet the load requirements [5]. A centralized TEG system needs to control only one maximum power point tracking (MPPT) controller, reducing hardware costs and making it easier to control the output voltage. However, the centralized TEG system has multiple peaks in the duty-power (D-P) characteristic curve at non-uniform temperature (NTD) and leads to a reduction in output power [6]. To improve the power output of the centralized TEG system, in this case, an adequate MPPT algorithm needs to be designed [7].

The associate editor coordinating the review of this manuscript and approving it for publication was Francesco Piccialli.

Traditional maximum power point tracking algorithms, in the form of Perturb and Observe (P&O) [8] and Incremental Conductance (INC) [9], have been used for a long time in temperature generation systems. However, the traditional MPPT algorithm has the disadvantage that it can easily fall into a local maximum power point (LMPP) with multiple power peaks. They are susceptible to environmental changes, with low reliability, which reduces the system's output power and will be limited in practical applications [10]. In addition, open-circuit voltage (OCV) and short-circuit current (SCC) methods are also commonly used in TEGs due to the approximately linear relationship between the open-circuit voltage V_{oc}, and the maximum operating voltage V_{MPP}, at a constant temperature [11], [12]. However, the relationship between V_{oc} and V_{MPP} is not linear, and the circuit requires periodic short-circuit or disconnect operations; these two methods cannot accurately track the MPP point and incur additional power loss [13].

In contrast, swarm intelligence algorithms have the advantages of simplicity and flexibility. Thankakan uses the particle swarm optimization (PSO) algorithm for MPPT control, which can efficiently find the global maximum power point (GMPP) under NTD. However, it is not easy to meet the TEG system to achieve fast MPPT requirements [14]. Compared with other swarm intelligence algorithms, Sparrow Search Algorithm (SSA), as an emerging intelligence algorithm, has higher convergence accuracy and better stability in test functions with multiple peaks [15].

In recent years, neural networks have become a research hotspot in artificial intelligence, which can simulate the human brain's response to the external environment and process complex information for modeling [16]. Currently, neural networks have been successfully applied in fields such as power forecasting [17] and pattern recognition [18]. Among them, Elman Neural Network (ENN) adds a connection layer to the BP neural network structure (input, hidden, and output layers), thus enhancing the global stability of the network, with short-term dynamic memory, which can be used to solve the fast optimization problem [19].

Based on the above discussion, this paper proposes an improved sparrow search algorithm with the Elman neural network for the maximum power point tracking of centralized thermoelectric generation systems under NTD. The algorithm fits the duty cycle and power curves by training samples and then uses the improved sparrow search algorithm to force the GMPP. Finally, we verify the effectiveness of the method through simulation experiments.

II. MODELING AND OUTPUT CHARACTERIZATION OF CENTRALIZED TEG SYSTEMS

A. TEG MODULE MODELING AND OUTPUT CHARACTERIZATION

The TEG module is one of the core components of centralized TEG systems, and establishing an accurate model of the TEG module is crucial for the performance analysis of the system. Due to the Seebeck effect formed by the difference between the hot end temperature T_h and cold end temperature T_c of the TEG module, the output of the TEG module generates a temperature difference electromotive force V_{oc}. The series connection of the voltage source V_{oc} with the internal resistance R_{in} is used to represent the ideal TEG module, whose value varies with the difference between T_h and T_c, as shown in Fig. 1.

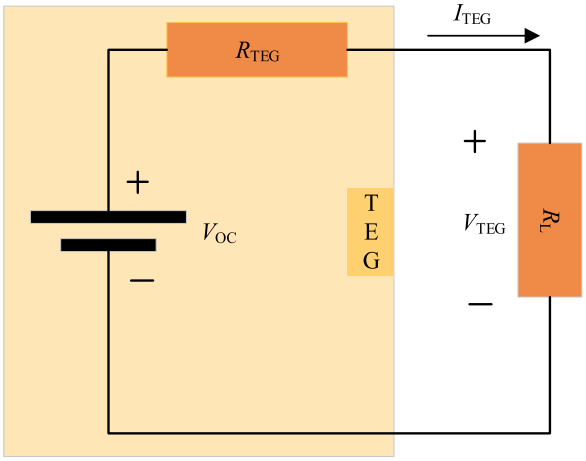

FIGURE 1. Equivalent circuit of the TEG module.

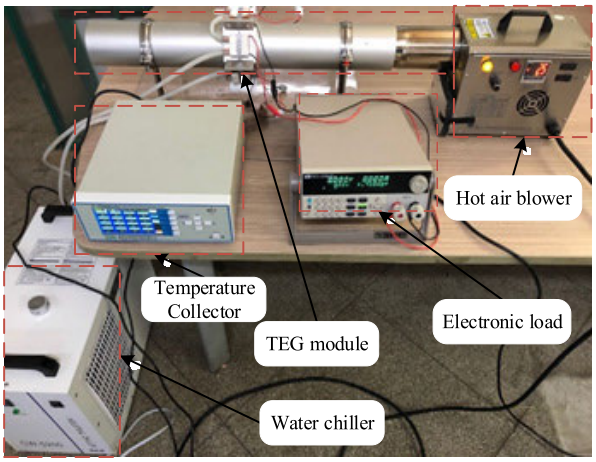

FIGURE 2. Experimental measurement platform.

This paper uses the TEP1-09656-0.5 TEG module produced by Jiangxi Nanometer Thermoelectric Electronic Co. Ltd. of China as the research object. It is a Bi-Te based TEG module that can operate continuously at heat source temperatures up to 310°C. In order to make the simulation model closer to reality, this study uses water chiller to keep the cold end temperature of the TEG module at 30°C, 40°C and 50°C, respectively, and then uses the high temperature air generated by Hot air blower to make the temperature of the hot end of the TEG module increase gradually, and measure its open-circuit voltage V_{oc} and resistance R_{in}. and the experimental measurement platform is shown in Fig. 2. The characteristic curves of V_{oc} and R_{in} versus the temperature of T_h are shown in Fig. 3.

We obtained the expressions of the corresponding V_{oc} and R_{in} fitting curves from the above characteristic curves of

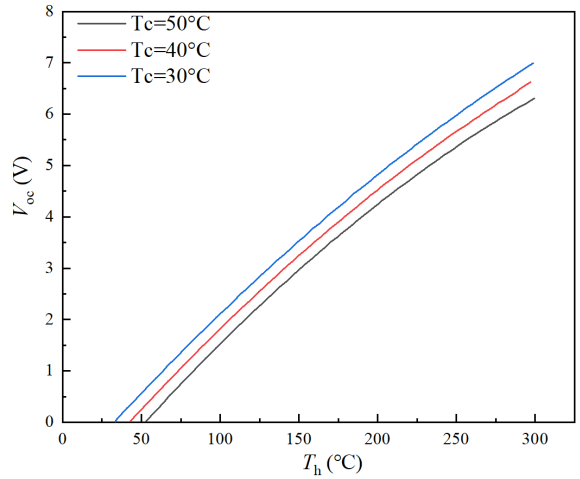

(a) The characteristic curve of V_{oc} and T_h

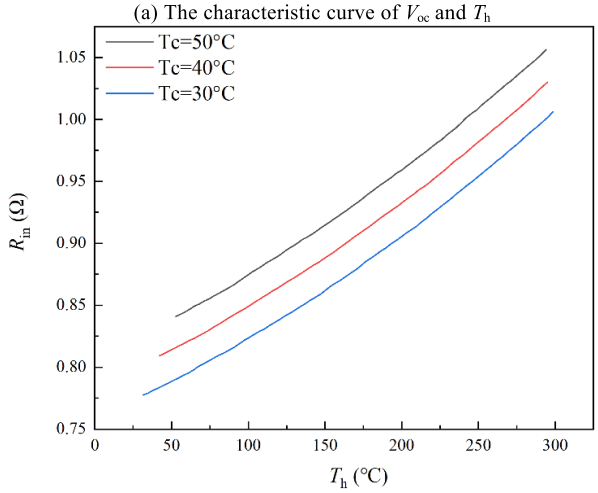

(b) The characteristic curve of R_{in} and T_h

FIGURE 3. Thermoelectric module output characteristic curve.

the open-circuit voltage and resistance versus the hot end temperature. We realized the dynamic correction of the simulation model parameters simultaneously, which creates the conditions for the subsequent verification of the property of the MPPT algorithm.

The expression for the fitted curve of the voltage source V_{oc} versus the internal resistance R_{in} for the TEG module at a cold end temperature of 50 °C is:

$$V_{oc} = -3.23499 \times 10^{-5} T_h^2 + 0.0369 T_h - 1.84137 \quad (1)$$

$$R_{TEG} = 9.05762 \times 10^{-7} T_h^2 + 5.79473 \times 10^{-4} T_h + 0.80749 \quad (2)$$

The expression for the fitted curve of the voltage source V_{oc} versus the internal resistance R_{in} for the TEG module at a cold end temperature of 40 °C is:

$$V_{oc} = -2.87021 \times 10^{-5} T_h^2 + 0.03568 T_h - 1.46384 \quad (3)$$

$$R_{TEG} = 9.31885 \times 10^{-7} T_h^2 + 5.58762 \times 10^{-4} T_h + 0.7838 \quad (4)$$

The expression for the fitted curve of the voltage source V_{OC} versus the internal resistance R_{in} for the TEG module at

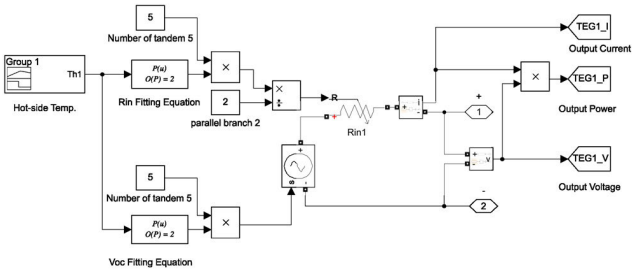

FIGURE 4. Thermoelectric module simulation model.

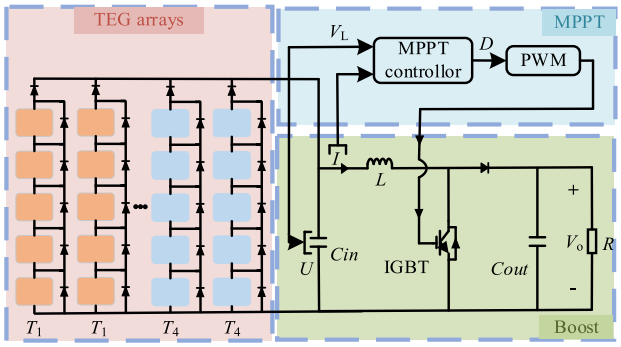

FIGURE 5. Centralized TEG system.

a cold end temperature of 30 °C is:

$$V_{oc} = -2.5522 \times 10^{-5} T_h^2 + 0.03475 T_h - 1.11001 \quad (5)$$

$$R_{TEG} = 9.39697 \times 10^{-7} T_h^2 + 5.44558 \times 10^{-4} T_h + 0.75922 \quad (6)$$

Based on the equivalent electrical model of the thermoelectric module and the expression of the parameter fitting curve, we built a simulation model in Simulink, and the simulation model is shown in Fig. 4.

B. TEG SYSTEM MODELING AND OUTPUT CHARACTERIZATION

The centralized thermoelectric generation system shown in Fig. 5 can be divided into three parts: the TEG array, the Boost circuit, and the MPPT controller. Among them, the TEG array consists of 40 TEG modules of model TEP1-09656-0.5 in 8 columns, with every two columns in a group and at the same temperature, and each column consists of 5 TEG modules connected in series. Under non-uniform temperature distribution, each TEG module also needs to be connected in parallel with a bypass diode to prevent the TEG module from operating at a reverse voltage; and a blocking diode is added at the end of each series to prevent reverse current from being generated by the voltage mismatch when the TEG series are connected in parallel. Since the internal resistance on the TEG array keeps changing with temperature, for load matching, we need to keep changing the duty cycle of the boost circuit.

The centralized TEG system model constructed using Matlab2020b/Simulink software is shown in Fig. 6. Among the parameters of the Boost circuit are: switching frequency

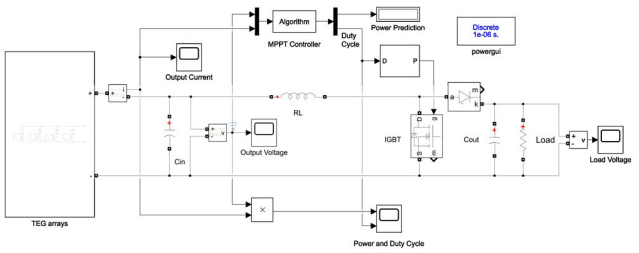

FIGURE 6. Centralized TEG system model.

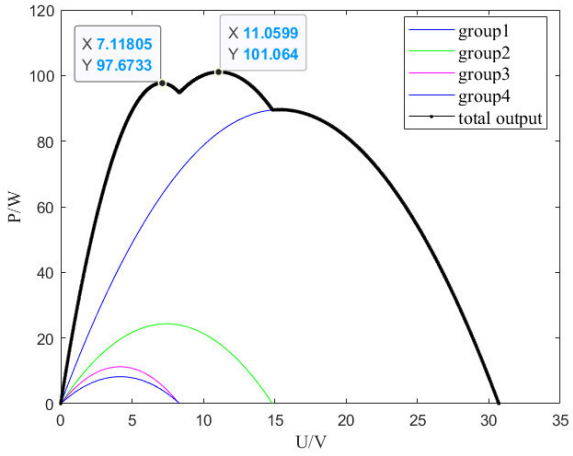

FIGURE 7. P-V curves of TEG arrays.

$f = 10$ kHz, input capacitance $C_{\text{in}} = 70\ \mu$F, $C_{\text{out}} = 330\ \mu$F, $L = 1.25$ mH, and load $R = 30\ \Omega$.

To simulate and study the effect of NTD on the output of the TEG array, the hot and cold ends of four groups of TEG strings are set to different temperatures in the simulation. The cold end temperatures of the four sets of TEG arrays are 50°C, 50°C, 40°C, and 30°C, and the hot end temperatures are 290°C, 140°C, 95°C, and 85°C, among others. Under the above working conditions, the *P-V* output curve of the whole TEG array is shown in Fig. 7 when the P-V output curve is multi-peaked.

III. MPPT CONTROL METHOD FOR TEG SYSTEM BASED ON ENN-ISSA ALGORITHM

A. ELMAN NEURAL NETWORK DESIGN

Different TEG system output powers can be obtained in a centralized TEG system by setting different boost converter duty cycles to get TEG system power output at any duty cycle. For the MPPT problem of the centralized TEG system, the output power of the TEG system is controlled by adjusting the duty cycle of the PWM signal of the MPPT controller. The relationship between the power output of the TEG system and the duty cycle of the MPPT controller cannot be represented by a simple function, so we can utilize the powerful nonlinear approximation capability of the Elman neural network to fit the complex functional relationship between the power output of the TEG system and the duty cycle of the MPPT controller. To realize the MPPT of the centralized TEG system, the input vector of the Elman neural network is set to the duty cycle of the MPPT controller, represented by $\boldsymbol{D}$, and the output vector

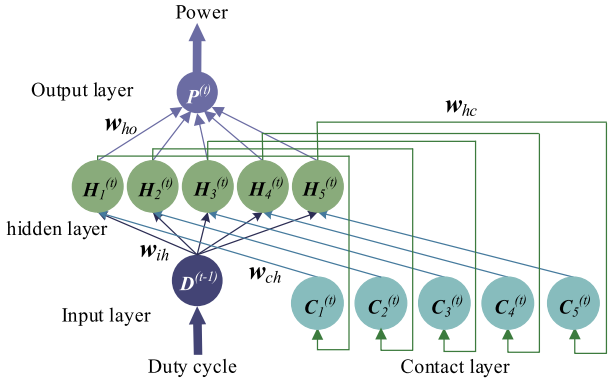

FIGURE 8. Elman neural network structure.

is set to the output power of the TEG system denoted by $\boldsymbol{P}$.

$$\boldsymbol{D} = \begin{bmatrix} D_1 \\ D_2 \\ \vdots \\ D_n \end{bmatrix} \quad \boldsymbol{P} = \begin{bmatrix} P_1 \\ P_2 \\ \vdots \\ P_n \end{bmatrix} \tag{7}$$

where $\boldsymbol{D}$ is the MPPT controller duty cycle vector, i.e., the ENN input layer input vector; $\boldsymbol{P}$ is the TEG system output power vector, i.e., the output layer output vector; and n is the number of training samples.

For the selection of the number of neurons in the hidden layer of the Elman neural network, we first derive an approximate range of the number of neurons in the hidden layer using the empirical formula commonly used to determine the number of neurons in the hidden layer, which is shown in (8). In this example, $n_o = n_i = 1$, and the n_{h} value ranges from a constant between 2 and 12. When the number of hidden layer neurons is 5, the mean square error MSE of the Elman neural network reaches the minimum value, and the number of hidden layer neurons is finally determined to be 5.

$$n_h < \sqrt{(n_o + n_i)} + \alpha \tag{8}$$

where n_h is the number of nodes in the hidden layer; n_o is the number of nodes in the output layer; n_i is the number of nodes in the input layer; and a is a constant between 0 and 10.

The Elman neural network can take the duty cycle of the MPPT controller and the power output from the TEG system and train a network to establish a mapping relationship between the duty cycle and the output power and the structure of the constructed Elman neural network is shown in Fig. 8.

Because the function Sigmoid is continuous and smooth everywhere, it is easy to derive, the transfer function of the hidden layer selects hyperbolic tangent Sigmoid function $f_{\text{h}}(z) = 2/(1+e^{-2z})-1$, and the transfer function of the output layer adopts the linear function Purelin. The mathematical model of the Elman neural network is as follows:

$$\begin{cases} \boldsymbol{H}_k^{(t)} = f_{\text{h}}\left(\boldsymbol{w}_{chk}\boldsymbol{C}_k^{(t)} + \boldsymbol{w}_{ihk}\boldsymbol{D}^{(t-1)} + \boldsymbol{b}_1\right) \\ \boldsymbol{C}_k^{(t)} = \boldsymbol{H}_k^{(t-1)} \\ \boldsymbol{P}^{(t)} = \sum \boldsymbol{w}_{hok}\boldsymbol{H}_k^{(t)} + \boldsymbol{b}_2 \end{cases} \tag{9}$$

where $\boldsymbol{H}_k^{(t)}$ is the kth hidden layer neuron output vector at moment t; $k = 1,2,\text{---},5$; $\boldsymbol{w}_{chk}$ is the weight between the kth connection layer and the kth hidden layer neuron; $\boldsymbol{C}_k^{(t)}$ is the kth connection layer neuron output vector at moment t; $\boldsymbol{w}_{ihk}$ is the weight between the input layer and the kth hidden layer neuron; $\boldsymbol{D}^{(t-1)}$ is the t-1 moment input layer input vector; $\boldsymbol{b}_1$ is the threshold of the kth hidden layer neuron; $\boldsymbol{P}^{(t)}$ is the output vector of the output layer at moment t; $\boldsymbol{w}_{hok}$ is the weight between the kth hidden layer neuron and the output layer; $\boldsymbol{b}_2$ is the threshold of the output layer.

The Elman neural network is used to fit the output power of the TEG system to the duty cycle of the boost converter. Its accuracy is not only related to the structure of the Elman neural network but to increase the representativeness and diversity of the initial samples, ten sets of data were uniformly selected within the range of DC/DC converter duty cycle variations [0, 0.95] to serve as the initial training samples for the duty cycle:

$$D_i = \frac{0.95}{10} i \quad i = 1, 2, \cdots, 10 \tag{10}$$

where D_i is the initial duty cycle of the ith training sample.

The duty cycles of these initial training samples are fed into the MPPT controller, where we can collect the corresponding voltage and current data from the TEG system and then normalize the output power of the TEG system for neural network pre-training. The training method is the Levenberg-Marquardt method.

By constantly updating each weight and threshold, the maximum number of training times of the Elman neural network is set to 50 times so that the mean square error between the expected power and the actual power of the training samples meets the predetermined error accuracy. The target mean square error of Elman neural network training is 0.001, and the formula for the prediction error accuracy is as follows:

$$E = \frac{1}{N} \sum_{i=1}^{N} \left(P_i - P_i'\right)^2 \tag{11}$$

where N is the number of duty cycles in the training samples; P_i is the output power of the TEG system corresponding to the ith duty cycle sample; P_i' is the power corresponding to the ith duty cycle sample predicted by the neural network.

B. BASIC SPARROW SEARCH ALGORITHM

The Sparrow Algorithm is a novel population intelligence algorithm proposed by the foraging and anti-predator behavior of sparrows. In this algorithm, the sparrow population is divided into discoverers and joiners. The discoverers search for food for the whole population and provide foraging directions for the joiners. The position update formula of the discoverer is:

$$X_{i,d}^{t+1} = \begin{cases} X_{i,d}^{t} \cdot \exp(\dfrac{-i}{\alpha * \mathrm{G}}), & R_2 < ST \\ X_{i,d}^{t} + Q \cdot L, & R_2 \geq ST \end{cases} \tag{12}$$

where t denotes the current number of iterations; $X_{i,d}^t$ represents the value of the dth dimension of the ith sparrow at the tth iteration; G is a constant that denotes the maximum value of the number of running iterations; α is a random number between (0,1]; R_2 takes values in the range of [0,1], and ST takes matters in the field of [0,5.1], which represent the warning value and safety threshold, respectively; Q is a random number that obeys a normal distribution; L denotes a $1 \times d$ matrix with 1 in each element. When $R_2 < ST$ means that the warning value is small and the predator is not nearby, indicating no risk of predation, $R_2 \geq ST$ implies that the warning value is significant, meaning that some of the sparrows detect the predator and there is a risk of predation. All other sparrows need to go to different places to forage for food.

The position update formula for joiners is as follows:

$$X_{i,d}^{t+1} = \begin{cases} Q \cdot \exp(\dfrac{X_{worst}^t - X_{i,d}^t}{i^2}), & i > \frac{n}{2} \\ X_P^{t+1} + \left|X_{worst}^t - X_{i,d}^t\right| \cdot A^+ \cdot L, & i \leq \frac{n}{2} \end{cases} \tag{13}$$

where X_P is the location of the finder that found the optimal food source; X_{worst} denotes the worst area of the current sparrow population; and A^+ represents a $1 \times d$ matrix where each element is randomly assigned a value of 1 or -1, and $A^+ = A^{\mathrm{T}}(AA^{\mathrm{T}})^{-1}$. When $i > n/2$, it indicates that the ith accession with the lower fitness value will need to fly elsewhere to forage.

To reduce the risk of sparrow predation, 10% to 20% of the sparrows from the sparrow population were selected as vigilantes with the following position update formula:

$$X_{i,d}^{t+1} = \begin{cases} X_{best}^t + \beta \cdot \left|X_{i,d}^t - X_{best}^t\right|, & f_i > f_g \\ X_{i,d}^t + K \cdot \dfrac{\left|X_{i,d}^t - X_{worst}^t\right|}{(f_i - f_g) + \varepsilon}, & f_i = f_g \end{cases} \tag{14}$$

In the formula, X_{best} is the current optimal position of the sparrow population; X_{worst} denotes the worst part of the current sparrow population; β is a random number obeying the standard Gaussian distribution; $K \in [-1,1]$ is a lucky number; f_i and f_g denote the global optimal and worst adaptation values, respectively; and ε is a very small constant avoiding the denominator to be 0. When fi > fg, it means that the sparrow is located in the edge position of the population and is easy to predate; when $f_i = f_g$, it means that the sparrow should approach other sparrows to get rid of the danger at this time.

C. FIREFLY PERTURBATION

Firefly perturbation is introduced to update the sparrow position and prevent the sparrow algorithm from prematurely falling into the local maximum power point. The firefly algorithm is a meta-heuristic algorithm proposed by Yang. This British scholar achieves the purpose of optimization through the idealized behavior of mutual attraction between individual fireflies in summer in the tropics. In the firefly algorithm, each firefly has a different brightness of the firefly at the location because of the different size of the fitness of

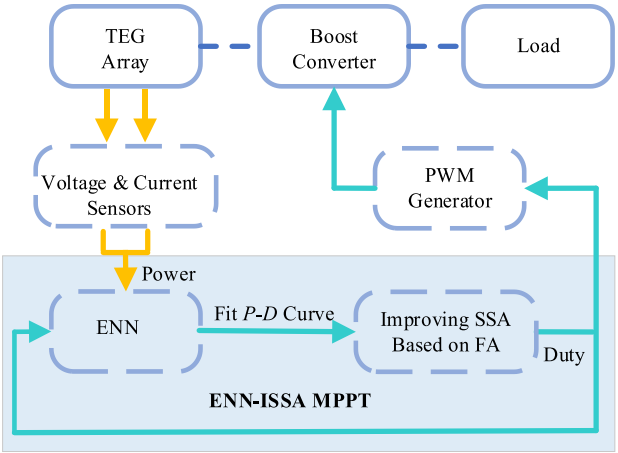

FIGURE 9. Solution for MPPT via ENN-ISSA.

its location, and the greater the brightness of the firefly, the greater the attraction, which attracts other fireflies with lower intelligence and causes the fireflies with lower brightness to approach it [20].

The attraction update formula between firefly individuals i and j is defined as:

$$\beta = \beta_0 e^{-\gamma r_{ij}^2} \tag{15}$$

where β_0 is the maximum attraction, i.e., the appeal of the firefly at the light source (at r = 0); γ is the light intensity absorption coefficient; and r_{ij} is the Cartesian distance from firefly i to firefly j.

The firefly individual i is attracted to j and moves toward it with the position update equation:

$$X_i = X_i + \beta(X_i - X_j) + \alpha_0 \varepsilon_0 \tag{16}$$

where X_i is the position of firefly i; X_j is the position of firefly j, i.e., the part of the brightest firefly; α_0 is usually a constant between 0 and 1, which is called the step-size control parameter; and ε_0 is a random number obeying a Gaussian distribution in the interval [0,1].

D. IMPLEMENTATION OF MPPT IN TEG SYSTEM

The scheme of realizing MPPT through ENN-ISSA in the TEG system is shown in Fig.9. First, the initial training samples' duty cycles are sent to the Boost converter. Then, the TEG system's voltage and current are measured, and the TEG system's power is normalized and used for pre-training the neural network. Second, ISSA searches the D-P curves that fit the initial training samples three times. Then, the three optimal duty cycles found by ISSA are added to the first training samples to reduce the mean square error between the desired power and the actual power of the ENN near the maximum power point. ISSA then looks for the best duty cycles to realize the MPPT.

The specific steps of the control process of the whole ENN-ISSA based MPPT control algorithm are as follows:

Step 1: Initialize the sparrow search parameters.

Step 2: Initialize the Elman neural network structure according to (9).

Step 3: The duty cycle samples used for training are initialized according to (10), and real-time voltages and currents are collected to calculate the output power corresponding to each initial duty cycle sample.

Step 4: Train the neural network using the Levenberg-Marquardt method and set the objective function for training according to (11).

Step 5: Start performing the sparrow search, calculate the power of each sparrow, that is, each duty cycle, and then sort the power magnitude to find the ''sparrow'' with the highest current power and the tiniest sparrow.

Step 6: Sparrows are ordered in order of power from largest to smallest, with a certain percentage of sparrows in front of them acting first as discoverers, whose positions are updated according to (12), and sparrows with less power working as joiners, whose positions are updated according to (13).

Step 7: A percentage of sparrows were randomly selected from the flock to act as vigilantes and their positions were updated according to (14).

Step 8: Introduce the firefly perturbation into the sparrow algorithm, update the position of the sparrows according to (16), and calculate the fitness value.

Step 9: If the termination condition is reached, obtain the current output best duty cycle D_b with the highest fitness value.

Step 10: The best duty cycle D_b input boost converter at the current moment in time is obtained by ISSA search.

Step 11: The corresponding voltages and currents are collected for each duty cycle of the TEG system, and the current power is calculated.

Step 12: Repeat steps 5 through 11 twice to add three new data samples to the neural network.

Step 13: Train the Elman neural network with the new training samples.

Step 14: Again, perform steps 5 through 10 to output the final optimal duty cycle D_b.

Step 15: The algorithm restarts when the output power of the TEG system changes $\Delta P > 4\%$.

IV. SIMULATION ANALYSIS

Since the algorithm parameters will impact the algorithms to find the optimal duty cycle, to ensure the fairness of the algorithm comparison, the standard parameters of different algorithms are set to be the same in this paper. The control period time of all algorithms is set to 0.02 s. We set the population of the ENN-ISSA algorithm and PSO algorithm to 5, and the initial positions of the individuals in the population are [0.1; 0.3; 0.5; 0.7; 0.9], respectively, and the maximum number of iterations is 10; when the number of algorithmic iterations reaches the set value, or the geometric positions of the two individuals in the population are is less than 0.1, or the maximum number of iterations is called. The distance between each individual in the population is less than 0.1, or the maximum number of iterations is reached.

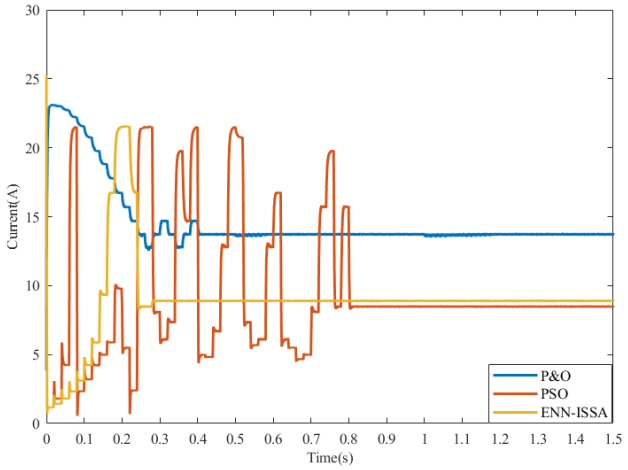

(a) Current waveform

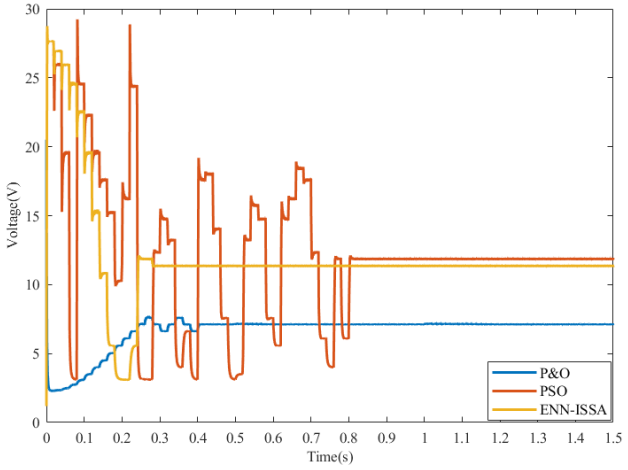

(b) Voltage waveform

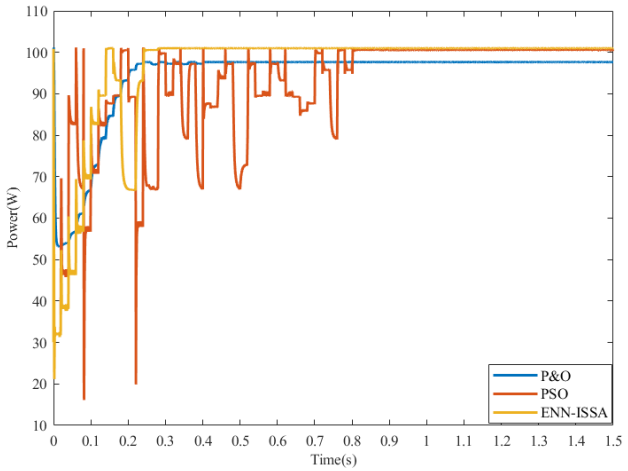

(c) Power waveform

FIGURE 10. Temperature constant experiment MPPT effect.

In addition, we set the P&O parameter to a fixed step size of 0.01, the PSO parameter to an inertia weight $w = 0.72$, and an acceleration coefficient $C_1 = C_2 = 1.52$; and we put the ENN-ISSA parameters to $\beta_0 = 1$, $\gamma = 1$, $\alpha_0 = 0.41$, discoverers proportion $PD = 0.6$, and vigilantes proportion $SD = 0.2$.

Change the size of the hot-side temperature in the Hot-side Temp module of Fig. 4, and substitute the expression of the fitted curve of the voltage source V_{oc} and the internal resistance R_{in} from the TEG module into the Voc Fitting Equation module and the Rin Fitting Equation module, so this system can realize the maximum power point tracking at different temperatures.

TABLE 1. Comparison of algorithm simulation results.

Method	Tracking Time	Achieved Power	Accurate
P&O	0.408s	97.645W	96.61%
PSO	0.812s	100.518W	99.46%
ENN-ISSA	0.285s	101.037W	99.97%

A. TEMPERATURE CONSTANCY EXPERIMENTS

The cold end temperatures of the four sets of TEG arrays are 50°C, 50°C, 40°C, and 30°C, and the hot end temperatures are 290°C, 140°C, 95°C, and 85°C, among others. The simulation results of the MPPT performance of the three algorithms under NTD are shown in Fig. 10.

From Fig. 7, the centralized TEG system's local maximum power point power at this temperature is 97.33 W. The global maximum power point power is 101.064 W. From Fig. 10, the P&O algorithm gets stuck in the LMPP, which results in the lowest output power of 97.66 W. Except for the P&O algorithm, both the ENN-ISSA algorithm and the PSO algorithm are less prone to fall into LMPP. As a result, the Elman neural network's nonlinear fitting function helps the ENN-ISSA algorithm shorten the algorithmic search time, significantly improves the convergence efficiency, and outputs a stable power of 101.037 W at 0.285 s. In the case of constant temperature, the ENN-ISSA algorithm realizes a fast and steady control of the maximum power point, and there are fewer oscillations during the search process.

B. SUDDEN TEMPERATURE CHANG EXPERIMENTS

In practice, the temperature of the hot end of the TEG array may change abruptly, so we set up four sets of temperature mutation experiments to observe whether the ENN-ISSA algorithm can track the GMPP quickly and accurately in the case of temperature mutation. The temperature mutation curve of the hot end of the TEG is shown in Fig. 11. The P-V output curves of the whole TEG array in the four sets of temperature sudden change experiments are shown in Fig. 12.

The performance simulation results of the three MPPT algorithms under temperature plunge are shown in Fig. 13. The simulation results show that the P&O algorithm quickly falls into the LMPP. The PSO algorithm can not obtain convergence speed and precision in the tracking process. At the second and fourth temperature plunges, it will fall into the local power point, although the convergence speed is fast. At the first and third temperature plunges, the PSO algorithm must go through a long time searching during the optimization process before it can finally approach the GMPP. In contrast, the ENN-ISSA algorithm can quickly track the GMPP when sudden temperature changes occur.

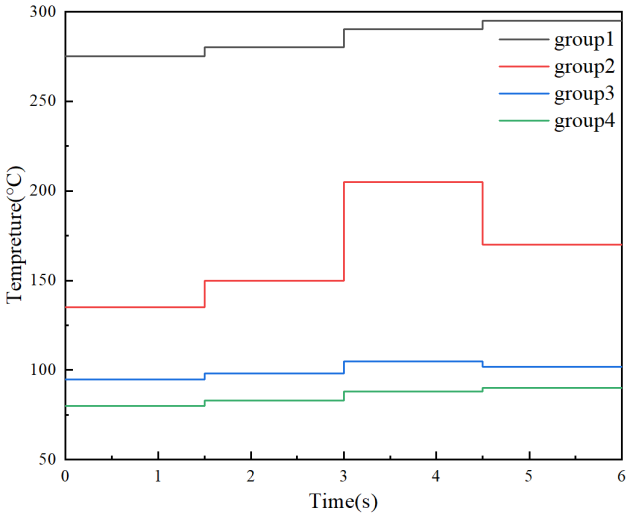

FIGURE 11. Temperature change at the hot end of a TEG string.

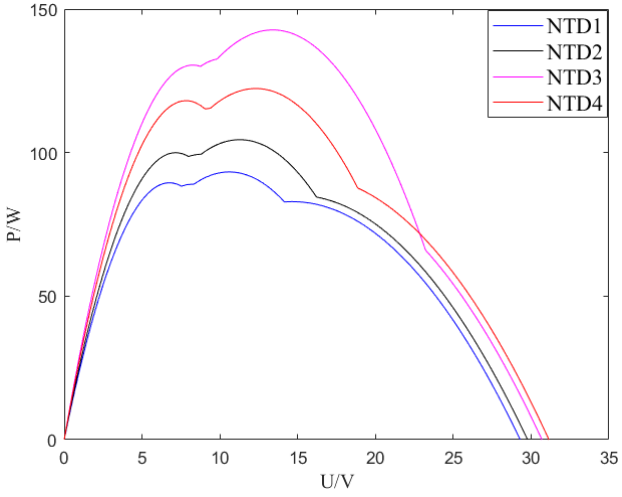

FIGURE 12. P-V curves of TEG arrays.

C. TIME-VARYING TEMPERATURE EXPERIMENT

In practical applications, the hot end temperature of the TEG string may change in real time in addition to sudden changes. The cold end temperatures of the four sets of TEG arrays are 50°C, 50°C, 40°C, and 30°C, and the hot end temperatures are 270°C, 110°C, 75°C, and 65°C, among others. The hot-side temperature of each group of TEG crossties started to increase at a rate of 2°C/s on top of the initial temperature at 1s and then began to decrease at a rate of 2°C/s at 6s until it remained unchanged after 9s.

The performance simulation results of the three MPPT algorithms under temperature time variation are shown in Fig. 14. Simulation results show that when the temperature changes in real-time, the P&O algorithm also stays around the LMPP, decreasing output power. The PSO algorithm has the slowest response, although it has a higher output power when the temperature changes in real time. The ENN-ISSA algorithm responds quickly to temperature variations and has the highest output power.

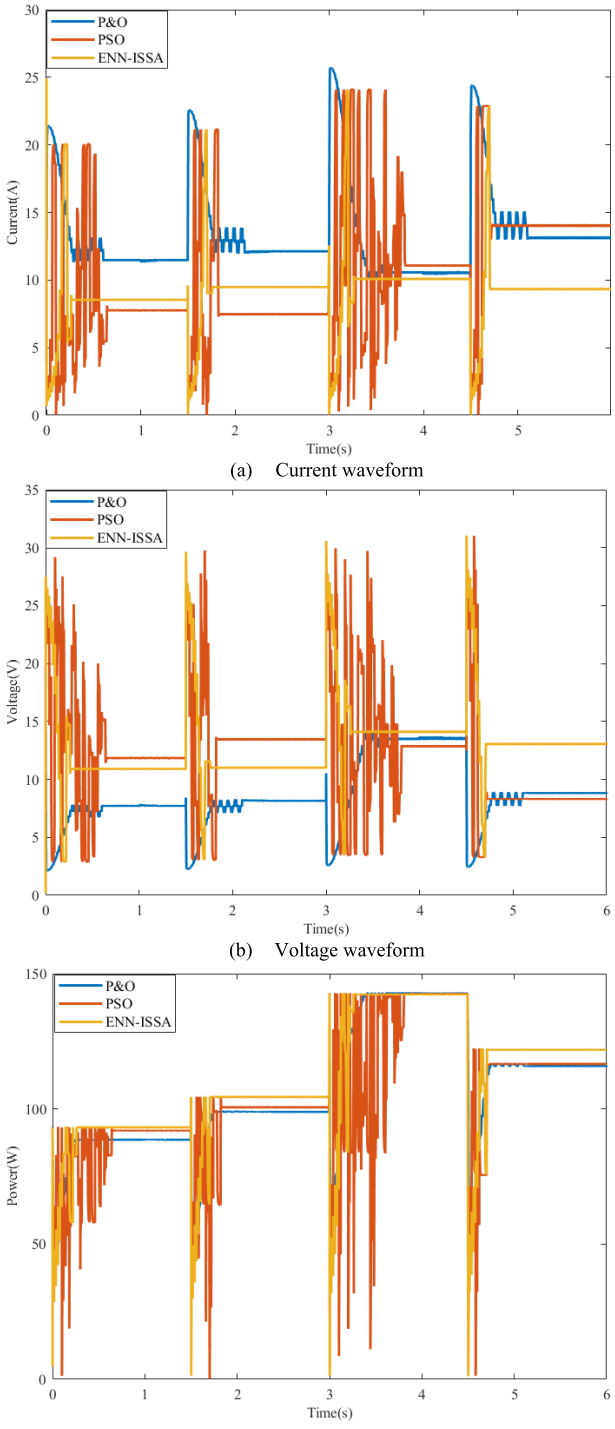

FIGURE 13. MPPT effect of temperature sudden change experiment.

D. ACCURACY ANALYSIS

Because the algorithms are randomized, 19 groups of different temperatures are set to test the tracking accuracy of different algorithms. The cold end temperature is maintained constant, and the hot end temperature is changed to ensure the temperature difference between the hot end and cold end is increased by 5% every time within the range of [10%, 100%] of the temperature difference set in the temperature constancy

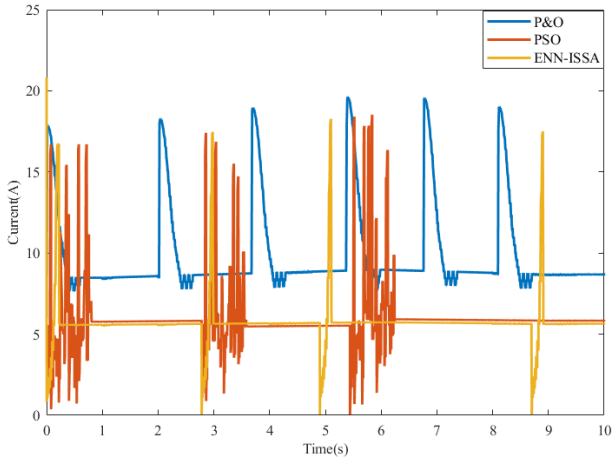

(a) Current waveform

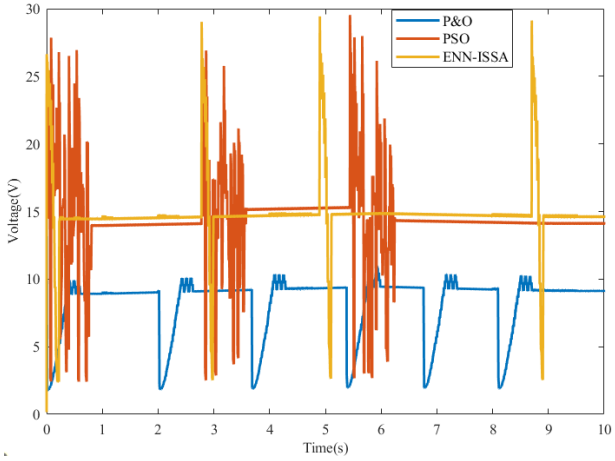

(b) Voltage waveform

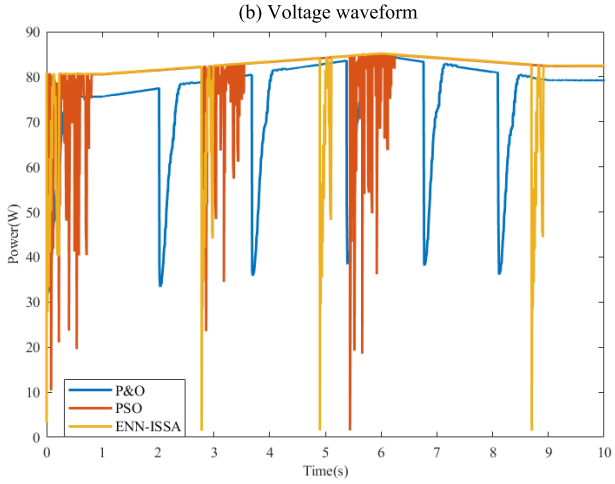

(c) Power waveform.

FIGURE 14. Temperature time-varying experiment MPPT effect.

experiments. The rated temperature settings of the cold end and hot end of each group of the TEG series are the same as those of the temperature constancy experiments. Fig. 15 shows the MPPT effect of the three methods for different temperature ratio experimental cases.

To quantitatively evaluate the tracking accuracy of each MPPT method in the set, the error evaluation indexes RMSE, MAE, and MAPE are introduced, and the results of the

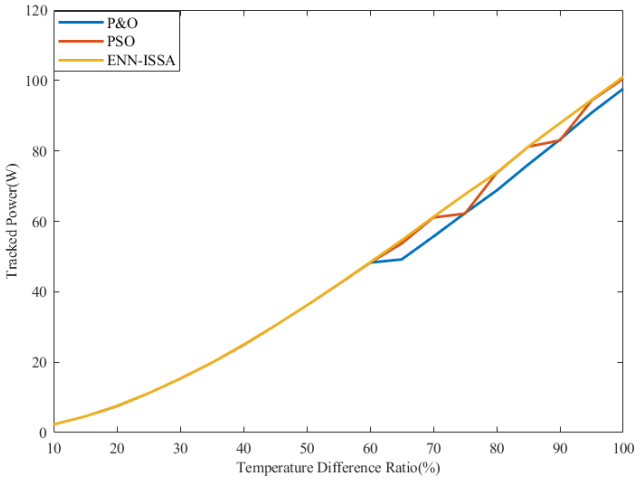

FIGURE 15. Accuracy analysis results.

TABLE 2. Calculation of error evaluation indicators.

Method	MSE	MAE	MAPE
P&O	10.0861	2.0521	2.98%
PSO	3.0333	0.7002	1.21%
ENN-ISSA	0.0034	0.7002	0.22%

calculation of the error evaluation indexes of each MPPT method are shown in Table 2.

$$MSE = \frac{1}{19}\sum_{i=1}^{19}\left(P^i_{\text{GMPP}} - P^i_{\text{Track}}\right)^2 \tag{17}$$

$$MAE = \frac{1}{19}\sum_{i=1}^{19}\left|\left(P^i_{\text{GMPP}} - P^i_{\text{Track}}\right)\right| \tag{18}$$

$$MAPE = \frac{100\%}{19}\sum_{i=1}^{19}\left|\frac{P^i_{\text{GMPP}} - P^i_{\text{Track}}}{P^i_{\text{GMPP}}}\right| \tag{19}$$

where P^i_{GMPP} is the power at the GMPP at the ith temperature difference, and P^i_{Track} is the power output from the TEG arrays after tracking by the MPPT algorithm at the ith temperature difference.

As seen in Fig. 15, the power tracked by each algorithm increases with the increase of the temperature difference ratio. The PSO algorithm falls into the LMPP when the temperature difference ratio is 75% and 90%. The PO algorithm always falls into the local maximum power point at the temperature difference ratio [65%,100%]. As can be seen in Table 2, the ENN-ISSA achieves the minimum value in the error evaluation indexes RMSE, MAE, and MAPE, which proves that ENN-ISSA has higher tracking accuracy and convergence stability than PSO algorithm and PO algorithm under different temperature difference ratios.

V. CONCLUSION

In this paper, for the problem that standard MPPT algorithms tend to fall into the LMPP or slow tracking speed under non-uniform temperature distribution, we propose to design

an algorithm based on the combination of the Elman neural network and the sparrow search with the introduction of firefly perturbation. ENN-ISSA utilizes Elman neural network to shorten the time of sampling duty cycle and power during the searching process of the MPPT algorithm and realizes the real-time control of MPPT. Then the firefly perturbation is introduced into the traditional SSA, which can effectively avoid falling into local optimality. Simulation experiments show that ENN-ISSA can track the GMPP under NTD fast and stably and is not affected by sudden temperature changes and real-time changes. Finally, the simulation results of accuracy analysis show that ENN-ISSA can effectively avoid falling into local optimality under 19 different temperature differences and has high tracking accuracy and convergence stability.

REFERENCES

[1] L. Gustavsson, T. Nguyen, R. Sathre, and U. Y. A. Tettey, "Climate effects of forestry and substitution of concrete buildings and fossil energy," *Renew. Sustain. Energy Rev.*, vol. 136, Feb. 2021, Art. no. 110435.
[2] X. He, F. Wang, T. J. Wallington, W. Shen, M. W. Melaina, H. C. Kim, R. De Kleine, T. Lin, S. Zhang, G. A. Keoleian, X. Lu, and Y. Wu, "Well-to-wheels emissions, costs, and feedstock potentials for light-duty hydrogen fuel cell vehicles in China in 2017 and 2030," *Renew. Sustain. Energy Rev.*, vol. 137, Mar. 2021, Art. no. 110477.
[3] A. M. Omer, "Focus on low carbon technologies: The positive solution," *Renew. Sustain. Energy Rev.*, vol. 12, no. 9, pp. 2331–2357, Dec. 2008.
[4] L. S. Hewawasam, A. S. Jayasena, M. M. M. Afnan, R. A. C. P. Ranasinghe, and M. A. Wijewardane, "Waste heat recovery from thermo-electric generators (TEGs)," *Energy Rep.*, vol. 6, pp. 474–479, Feb. 2020.
[5] A. Montecucco, J. Siviter, and A. R. Knox, "The effect of temperature mismatch on thermoelectric generators electrically connected in series and parallel," *Appl. Energy*, vol. 123, pp. 47–54, Jun. 2014.
[6] C. Yu and K. T. Chau, "Thermoelectric automotive waste heat energy recovery using maximum power point tracking," *Energy Convers. Manage.*, vol. 50, no. 6, pp. 1506–1512, Jun. 2009.
[7] W. He, G. Zhang, X. Zhang, J. Ji, G. Li, and X. Zhao, "Recent development and application of thermoelectric generator and cooler," *Appl. Energy*, vol. 143, pp. 1–25, Apr. 2015.
[8] H. Mamur and R. Ahiska, "Application of a DC–DC boost converter with maximum power point tracking for low power thermoelectric generators," *Energy Convers. Manage.*, vol. 97, pp. 265–272, Jun. 2015.
[9] R.-Y. Kim, J.-S. Lai, B. York, and A. Koran, "Analysis and design of maximum power point tracking scheme for thermoelectric battery energy storage system," *IEEE Trans. Ind. Electron.*, vol. 56, no. 9, pp. 3709–3716, Sep. 2009.
[10] N. Femia, G. Petrone, G. Spagnuolo, and M. Vitelli, "Optimization of perturb and observe maximum power point tracking method," *IEEE Trans. Power Electron.*, vol. 20, no. 4, pp. 963–973, Jul. 2005.
[11] A. Montecucco and A. R. Knox, "Maximum power point tracking converter based on the open-circuit voltage method for thermoelectric generators," *IEEE Trans. Power Electron.*, vol. 30, no. 2, pp. 828–839, Feb. 2015.
[12] M. Bond and J.-D. Park, "Current-sensorless power estimation and MPPT implementation for thermoelectric generators," *IEEE Trans. Ind. Electron.*, vol. 62, no. 9, pp. 5539–5548, Sep. 2015.
[13] H. Mamur, M. A. Üstüner, and M. R. A. Bhuiyan, "Future perspective and current situation of maximum power point tracking methods in thermoelectric generators," *Sustain. Energy Technol. Assessments*, vol. 50, Mar. 2022, Art. no. 101824.
[14] R. Thankakan and E. R. Samuel Nadar, "Investigation of the double input power converter with N stages of voltage multiplier using PSO-based MPPT technique for the thermoelectric energy harvesting system," *Int. J. Circuit Theory Appl.*, vol. 48, no. 3, pp. 435–448, Mar. 2020.
[15] J. Xue and B. Shen, "A novel swarm intelligence optimization approach: Sparrow search algorithm," *Syst. Sci. Control Eng.*, vol. 8, no. 1, pp. 22–34, Jan. 2020.
[16] M. Nikzad, K. Movagharnejad, and F. Talebnia, "Comparative study between neural network model and mathematical models for prediction of glucose concentration during enzymatic hydrolysis," *Int. J. Comput. Appl.*, vol. 56, no. 1, pp. 1–6, 2012.
[17] S. Al-Dahidi, O. Ayadi, M. Alrbai, and J. Adeeb, "Ensemble approach of optimized artificial neural networks for solar photovoltaic power prediction," *IEEE Access*, vol. 7, pp. 81741–81758, 2019.
[18] O. I. Abiodun, A. Jantan, A. E. Omolara, K. V. Dada, A. M. Umar, O. U. Linus, H. Arshad, A. A. Kazaure, U. Gana, and M. U. Kiru, "Comprehensive review of artificial neural network applications to pattern recognition," *IEEE Access*, vol. 7, pp. 158820–158846, 2019.
[19] J. L. Elman, "Finding structure in time," *Cognit. Sci.*, vol. 14, no. 2, pp. 179–211, Mar. 1990.
[20] S. Mohammadi, B. Mozafari, S. Solimani, and T. Niknam, "An adaptive modified firefly optimisation algorithm based on Hong's point estimate method to optimal operation management in a microgrid with consideration of uncertainties," *Energy*, vol. 51, pp. 339–348, Mar. 2013.

XINYING HE was born in Nanchong, Sichuan, in 2000. She is currently pursuing the master's degree in electrical engineering with the Taiyuan University of Technology, Shanxi, China. Her main research interest includes research on temperature difference power generation and its control.

YAN CHEN was born in Shuozhou, Shanxi, in 1977. She received the Ph.D. degree in circuits and systems from the Taiyuan University of Technology, China, in 2011. She is currently with the Electrical Machines Department, School of Electrical and Power Engineering, China Taiyuan University of Technology. Her current research interests include power electronics and power transmission, special motor drives and their automation, intelligent information processing, and new energy generation technology.

QIAN DU was born in Xinzhou, Shanxi, in 1997. He received the B.S. degree in electrical engineering from the Taiyuan University of Technology, Shanxi, China, in 2023. He is currently pursuing the Ph.D. degree with the Taiyuan University of Technology, China. His research interests include new energy generation technology, power electronics, and power transmission.

LULU FENG was born in Linfen, Shanxi, in 2000. He is currently pursuing the master's degree in electrical engineering with the Taiyuan University of Technology, Shanxi, China. His main research interest includes new energy generation technology.